



HAL
open science

Bond Graph modeling for fault detection and isolation of a train door mechatronic system

Laurent Cauffriez, Sébastien Grondel, Pierre Loslever, Christophe Aubrun

► **To cite this version:**

Laurent Cauffriez, Sébastien Grondel, Pierre Loslever, Christophe Aubrun. Bond Graph modeling for fault detection and isolation of a train door mechatronic system. *Control Engineering Practice*, 2016, 49, pp.212-224. 10.1016/j.conengprac.2015.12.019 . hal-01293364

HAL Id: hal-01293364

<https://hal.science/hal-01293364v1>

Submitted on 30 Sep 2024

HAL is a multi-disciplinary open access archive for the deposit and dissemination of scientific research documents, whether they are published or not. The documents may come from teaching and research institutions in France or abroad, or from public or private research centers.

L'archive ouverte pluridisciplinaire **HAL**, est destinée au dépôt et à la diffusion de documents scientifiques de niveau recherche, publiés ou non, émanant des établissements d'enseignement et de recherche français ou étrangers, des laboratoires publics ou privés.

Bond Graph modeling for fault detection and isolation of a train door mechatronic system

Laurent Cauffriez ^{a,*}, Sébastien Grondel ^b, Pierre Loslever ^a, Christophe Aubrun ^c

^a LAMIH, UMR CNRS 8201, Université de Valenciennes, Le Mont Houy, F-59313 Valenciennes Cedex 9, France

^b IEMN-DOAE, UMR CNRS 8520, Université de Valenciennes, Le Mont Houy, F-59313 Valenciennes Cedex 9, France

^c CRAN, UMR CNRS 7039, Université de Lorraine, Campus Sciences, F-54506 Vandoeuvre Cedex, France

Keywords:

Bond Graph
Train door
Mechatronic system
Fault detection and isolation
Residuals

abstract

In this paper, monitoring and diagnosis of a new generation of train door mechatronic system is proposed. Bond Graph methodology is applied to obtain a reference model. In addition to this reference model, a global model based-FDI (Fault Diagnostic and Isolation) is developed for the generation of fault indicators and residual thresholds in presence of door failures. The ability of the proposed diagnostic approach to detect train door failures is demonstrated. The main contribution of this paper concerns the implementation of FDI procedure on a train door instead of health monitoring as it is usually performed in maintenance field.

1. Introduction

Technical processes are becoming more and more complex and if a fault occurs, safety may severely be affected, particularly in processes like aircraft, trains, automobiles, power plants and chemical plants (Isermann, 2005; Chen & Patton, 1999). Consequently, Fault Detection and Isolation (FDI) domain has received considerable attention during the last three decades (Patton, Franck & Clark, 2000).

FDI approaches are usually divided in two categories: data-driven and model-based methods. Successful applications of the data-driven FDI methods, in particular the multivariate analysis methods, have recently been reported in the process industry (Venkatasubramanian, Rengaswamy & Kavuri, 2003). The wide integration of powerful Supervisory Control And Data Acquisition (SCADA) systems has also promoted this development. Compared with the model-based FDI schemes, the performance of the data-driven methods is often limited in dealing with dynamic processes and FDI in feedback control loops. Also, most of the reported FDI applications are at the process component level, and limited to these “small-scale” processes (e.g., up to hundred sensors and actuators).

Model-based fault detection includes residual generation and residual evaluation (Svard, Nyberg, Frisk & Krysander, 2014). The major efforts in this area have been dedicated to the FDI in Linear Time Invariant (LTI) systems. As a result, a theoretical framework for design and analysis is well established (Isermann, 2006; Blanke, Kinnaert, Lunze & Staroswiecki, 2006; Ding, 2008). Lately, special attention has been given to fault detection approaches for Linear Parameters Varying (LPV) systems (Ponsart, Theilliol & Aubrun, 2010; Varga & Ossmann, 2014; Nazari, Seron & De Doná, 2013; Henry, 2013).

The current research focus in this area is on robustness (Keliris, Polycarpou & Parisini, 2015), nonlinear and hybrid system issues (Ding, 2008). In the past, efforts have also been made to extend the existing model-based FDI methodology to deal with problems in decentralized control systems (Mehiged, Yamé & Aubrun, 2010). Research has been carried out on those processes which are well modeled as interconnected LTI-subsystems, and the diagnosis is dedicated to the system components (Chun, Speyer & Chen, 2001; Yan & Edwards, 2007; Li, Gui, Xie & Ding, 2009).

Recently, model-based approaches have been successfully applied on railway system. A robust observer-based filter has been developed for a single-phase Pulse Width Modulated (PWM) rectifier for electric railway traction systems in (Youssef, El Khil & Slama-Belkhdja, 2013). An extended Kalman filter and a Luenberger observer have been investigated for electric vehicle power trains, and for a permanent magnet synchronous motors drive for faulty position or speed sensors in (Akrad, Hilarait & Diallo, 2011). Finally, (Dassanayake, Roberts, Goodman & Tobias, 2009) are the

* Corresponding author.

E-mail addresses: Laurent.Cauffriez@univ-valenciennes.fr (L. Cauffriez), Sebastien.Grondel@univ-valenciennes.fr (S. Grondel), Pierre.Loslever@univ-valenciennes.fr (P. Loslever), Christophe.Aubrun@univ-lorraine.fr (C. Aubrun).

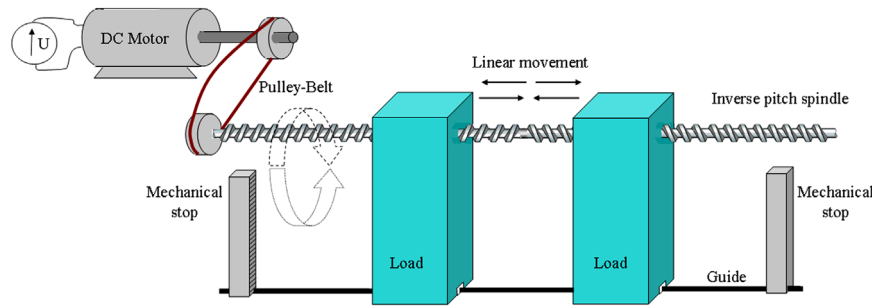


Fig. 1. Description of the mechatronic system.

only one to use parameter estimation for the detection and diagnosis of faults on electric train door systems. However, obtaining an accurate analytical model may be difficult in practice.

An alternative approach consists in establishing a Bond Graph model. Bond Graph modeling is a systematic method for modeling dynamic systems with different energy domains (Paynter, 1959; Borutzky, 2011; Mezghanni, Andoulsi, Mami & Dauphin-Tanguy, 2007), such as electrical, mechanical and hydraulic systems, in a unified framework. Bond Graph is quite intuitive since it is based on the energy conservation principle that generates system equations and graphical representation which facilitate design of FDI algorithms (Rosenberg & Karnopp, 1972).

In the recent research on the FDI of railway system, a fault monitoring framework based on combined use of data-driven and Bond Graph modeling for a locomotive electro-pneumatic brake has been developed in (Niu, Zhao, Defoort & Pecht, 2015).

Statistical studies reported in (Turgis, Copin, Loslever, Cauffriez & Caouder, 2009; Cauffriez, Loslever, Caouder, Turgis & Copin, 2013) point out that doors are responsible from 30% to 40% of the failures in commercial use. This is a problematic area that train manufacturers have to consider as it leads to societal and economical impacts. In particular, it implies not only costs due to delays but also financial penalties that must be paid by the train manufacturer to the railway operator. One of the major reasons is related to the current diagnosis of faulty doors which is made offline and outboard by the maintenance center and results in files containing a high amount of alarms and data. Therefore, this is an approach that takes time and for which it is difficult to find the cause of failures.

Within this context, the aim of this paper is to propose a solution to facilitate the detection and analysis of the door failures. The chosen approach deals with the introduction of a model-based FDI (Fault Detection and Isolation) in addition to the urban train reference model for the generation of fault indicators and residuals thresholds in presence of door failures.

As the modeling of train doors involves several domains of energy, the Bond Graph has been chosen for this study. Among the other multiple benefits provided by the Bond Graph formalism, it allows both causal and behavioral process analysis (Gawthrop, 1991; Borutzky, Dauphin-Tanguy & Thoma, 1995) and it is a graphical tool well adapted for diagnosis (Merzouki, Medjaher, Djéziri & Ould-Bouamama, 2007; Ould Bouamama, Medjaher, Bayart, Samantaray & Conrard, 2005; Samantaray, Medjaher, Ould Bouamama, Staroswiecki & Dauphin-Tanguy, 2006; Roberts, Balance & Gawthrop, 1995; Samantaray & Ghoshal, 2008). Compared to the conventional modeling approaches, the use of Bond Graph model allows dealing with structural control properties (controllability, observability, and invertibility) that are deduced from the causality relationships between causes and effects. Analysis of causal paths can identify problems in formulation of the model equations and also problems than one may face in numerical evaluations. Furthermore, causal properties of the Bond Graph model have been

used to determine the origin of the consequences of the faults.

This article can be divided into four parts. First, a reference model for the modeling of the well-functioning of a train door mechatronic system is proposed in Section 2. Section 3 is dedicated to the analysis of current and position signals directly measured on a test bench in order to characterize real train doors behavior and to validate the reference model. Then a global model-based FDI is detailed in Section 4 and contributions to fault detection and isolation are developed. Section 5 focuses on simulation results for the characterization of residuals for certain internal and external failures of the train door. Finally, conclusions about this research work are given, pointing out the ability to detect internal and external failures for the proposed model-based FDI.

2. System reference model

2.1. Mechatronic system description

Fig. 1 illustrates the train door mechatronic system that can be naturally divided in five sub-systems:

1. The input voltage source U .
2. The Direct Current DC motor.
3. The Pulley-Belt PB.
4. The inverse Pitch Spindle S .
5. The load parts and guide.

Regarding its functioning, a positive (or a negative) value of the input voltage source U leads to a clockwise (anticlockwise) rotation of the “Pulley-Belt /inverse Pitch Spindle” subsystem resulting in a linear movement of load parts. Thus, both load parts are approaching or moving away depending on the direction rotation of the motor. Finally, the guide ensures a longitudinal displacement of loads until mechanical stops are reached.

2.2. Bond Graph modeling

Usually, the Bond Graph modeling requires first establishing the Word Bond Graph of the system. As this representation is a first level toward the energy map description of the system and its composition, a physical analysis of the system and its power interaction are sufficient to determine it. From Fig. 1, it makes sense to decompose the Word Bond Graph into 5 subsystems as shown in Fig. 2. Contrary to the classical block diagrams, the inputs and outputs of each subsystem define here power variables represented by a conjugated pair of effort-flow (e,f) labeled by a half arrow. For this specific application, power variables used are the followings:

$$(Voltage, current) = (U, i) \quad (1)$$

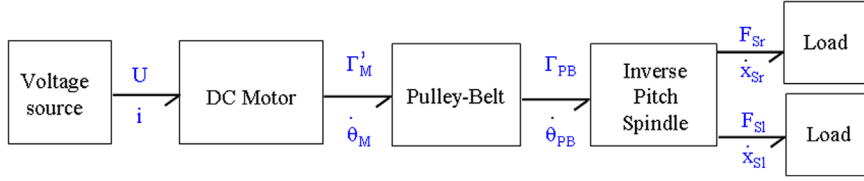


Fig. 2. Word Bond Graph.

$$(\text{Torque, angular velocity}) = (\Gamma'_M, \dot{\theta}_M); (\Gamma_{PB}, \dot{\theta}_{PB}) \quad (2)$$

$$(\text{Force, linear velocity}) = (F_{Sr}, \dot{x}_{Sr}); (F_{Sl}, \dot{x}_{Sl}) \quad (3)$$

As a result, electrical and mechanical aspects (including both rotation and translation) of the physical system are respectively modeled by these variables which allow the study of power exchange inside it.

Once the word Bond Graph is obtained, the next step consists in describing the Bond Graph of each subsystem from the equations involving the electrical and mechanical variables. It should be reminded that a Bond Graph is composed of basic elements associated with ports: I and C are used for kinetic and potential energy storage, R for energy dissipation, ports Se and Sf as sources of efforts and flows. Furthermore, elements 0 , 1 , TF (transformer), GY (gyrator) compose the junction structure, with exchanges energy between the difference parts of the dynamic system and which is constrained to satisfy power conservation.

2.2.1. Modeling of the motor subsystem and the associated voltage source

In the present modeling, the DC motor can be divided in two parts. The first part consists in an electrical $R_M L_M$ circuit (R_M : resistance, L_M : inductance) powered by a voltage source U as well as a back electromagnetic force characterized by a linearly dependence with the motor shaft angular velocity $\dot{\theta}_M$, ke being the constant motor's back electromagnetic force. This part is actually described by the following equation:

$$U = L_M \frac{di}{dt} + R_M i + ke \cdot \dot{\theta}_M \quad (4)$$

The second part corresponds to the mechanical side (see Eq. (5)). It includes the rotational moment of the motor inertia J_M , a control motor torque input Γ_M , a frictional torque Γ_R equal to the term $B_M \cdot \dot{\theta}_M$ (B_M being the viscous friction) and Γ'_M which represents the torque of the motor once connected to the Pulley-Belt subsystem.

$$J_M \cdot \ddot{\theta}_M = \Gamma_M - B_M \cdot \dot{\theta}_M - \Gamma'_M \quad (5)$$

From Eqs. (4) and (5), it is easy to deduce the Bond Graph model of the DC motor and its voltage source (see Fig. 3). As a reminder, 1-junction in a Bond Graph model represents a node at which all flows of the connecting bonds are equal and at which the efforts sum is zero. In electrical networks, this summation corresponds to the Kirchhoff voltage law (see Eq. (4)) whereas it represents a force balance (also called the d'Alembert's principle) in the mechanical domain and is a generalization of the Newton's third law.

It can be noticed that this Bond Graph model contains both an electrical part and a rotation mechanical part. The electrical part consists in a modulated voltage source ($MSe:U$), a resistor dissipating free energy ($R:R_M$), a storage element i.e. an inductor ($I:L_M$) and a gyrator corresponding to the electrical port of the DC motor ($GY:ke$). The rotation mechanical domain includes the rotation port of the DC motor ($GY:ke$), a resistor dissipating free energy i.e. viscous friction ($R:B_M$) and a storage element i.e. inertia ($I:J_M$).

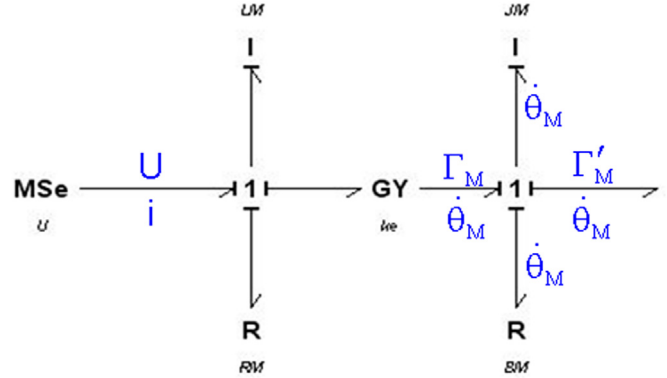


Fig. 3. Bond Graph model of DC motor and its voltage source.

2.2.2. Modeling of Pulley-Belt subsystem

In the studied system, the role of the Pulley-Belt part is to link its velocity $\dot{\theta}_{PB}$ with the mechanical motor axis velocity $\dot{\theta}_M$ such as:

$$\dot{\theta}_{PB} = N_{M1} \cdot N_{M2} \cdot \dot{\theta}_M - \frac{1}{k_{PB}} \cdot N_{M2}^2 \cdot \frac{d\Gamma_{PB}}{dt} \quad (6)$$

where Γ_{PB} represents the torque of the Pulley-Belt.

Following the same procedure as that of the previous section, the Pulley-Belt subsystem is modeled by two ideal transformer elements TF where power is continuous (i.e. no power is stored or dissipated) (Amerongen, 2003) and a storage element i.e. the elastic translational coefficient of the belt ($C:1/k_{PB}$). Due to the power continuity, dimensionless parameters N_{M1} and N_{M2} are needed to describe both the effort transduction and the flow transduction. Fig. 4 gives the corresponding Bond Graph model. As a reminder, 0-junction in a Bond Graph model represents a node at which all efforts of the connecting bonds are equal and at which the flow sum is zero.

2.2.3. Modeling of inverse Pitch Spindle subsystem

This section describes the inverse Pitch Spindle subsystem which is represented by its inertia J_S , a viscous friction coefficient B_S and the rotation to linear transformation of the right N_{Sr} and left N_{Sl} load parts. Furthermore, F_{Sr} and F_{Sl} in the following equations correspond to the left and right load charges applied to the inverse Pitch Spindle subsystem.

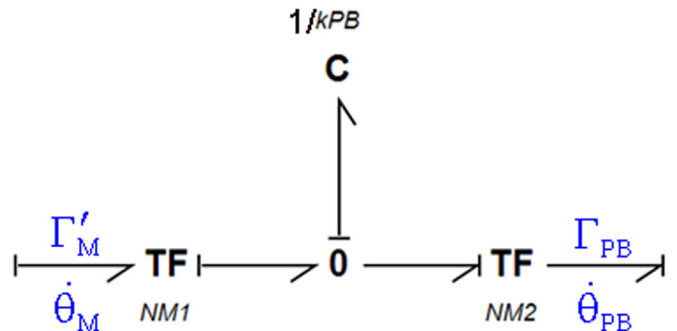


Fig. 4. Bond Graph model of Pulley-Belt subsystem.

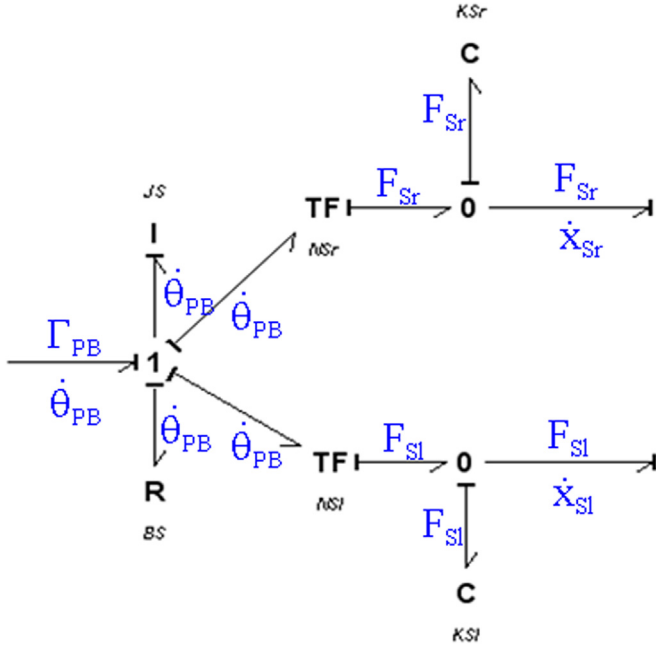


Fig. 5. Bond Graph model of Inverse Pitch Spindle subsystem.

$$\begin{cases} J_S \cdot \ddot{\theta}_{PB} = \Gamma_{PB} - B_S \cdot \dot{\theta}_{PB} - N_{Sr} \cdot F_{Sr} - N_{Sl} \cdot F_{Sl} \\ \dot{x}_{Sr} = N_{Sr} \cdot \dot{\theta}_{PB} - \frac{1}{k_{Sr}} \cdot \frac{dF_{Sr}}{dt} \\ \dot{x}_{Sl} = N_{Sl} \cdot \dot{\theta}_{PB} - \frac{1}{k_{Sl}} \cdot \frac{dF_{Sl}}{dt} \end{cases} \quad (7)$$

Then, the Bond Graph model of the inverse Pitch Spindle can be deduced from Eq. (7) (see Fig. 5). It consists in a resistor dissipating free energy i.e. viscous friction ($R:B_S$), a first storage element linked to the inertia of the inverse Pitch Spindle ($I:J_S$), two others storage elements due to the “spindle-load” elasticity coefficients ($C:1/k_{Sr}$, $C:1/k_{Sl}$) and finally two ideal transformer elements ($TF:N_{Sr}$, $TF:N_{Sl}$) corresponding to the rotation to linear transformations.

2.2.4. Modeling of load parts

In the same way, load parts are modeled by a set of forces i.e. the inertial forces through the M_r and M_l masses as well as the frictions forces through the B_r and B_l viscous friction coefficients. It can also be noticed also that external friction forces F_r and F_l correspond to a variation of the Stribeck friction effect together with the static friction (dry friction) effect. The dry friction effect is approximated by a combination of a switch model and the dry friction model (Jang & Jeon, 2000). Thus, depending on the conditions on \dot{x}_{Sr} , F_{Sr} , Dv (which is a sensitivity threshold), the friction force F_r for the right load part is equal to:

- i) Stick: if $(|\dot{x}_{Sl}| < Dv)$ and $(|F_{Sl}| \leq \mu_0 \cdot M_r \cdot g)$ then $F_r = F_{Sr}$
- ii) Stick-to-slip: if $(|\dot{x}_{Sl}| < Dv)$ and $(|F_{Sl}| > \mu_0 \cdot M_r \cdot g)$ then $F_r = \mu_0 \cdot M_r \cdot g \cdot \text{sgn}(\dot{x}_{Sr})$
- iii) Slip: if $(|\dot{x}_{Sl}| \geq Dv)$ then $F_r = \mu_0 \cdot M_r \cdot g \cdot \text{sgn}(\dot{x}_{Sr})$

where sgn is the sign function, μ_0 represents a constant friction coefficient due to the linear motion of the train door on the guide, M_r is the mass of the right load part and g corresponds to the standard gravity constant. It is to be noted that the friction force F_l for the left load part can be simply deduced by substituting in Eq. (8) \dot{x}_{Sr} , F_{Sr} , F_r respectively by \dot{x}_{Sl} , F_{Sl} , F_l .

Besides, mechanical stops are added in the model to restrict the motion of the loads (see Fig. 1). More precisely, they are firstly modeled by hard springs k_{MSr} and k_{MSl} and dampers B_{MSr} and B_{MSl} , and secondly triggered by the Tr and Tl logic elements. As a result,

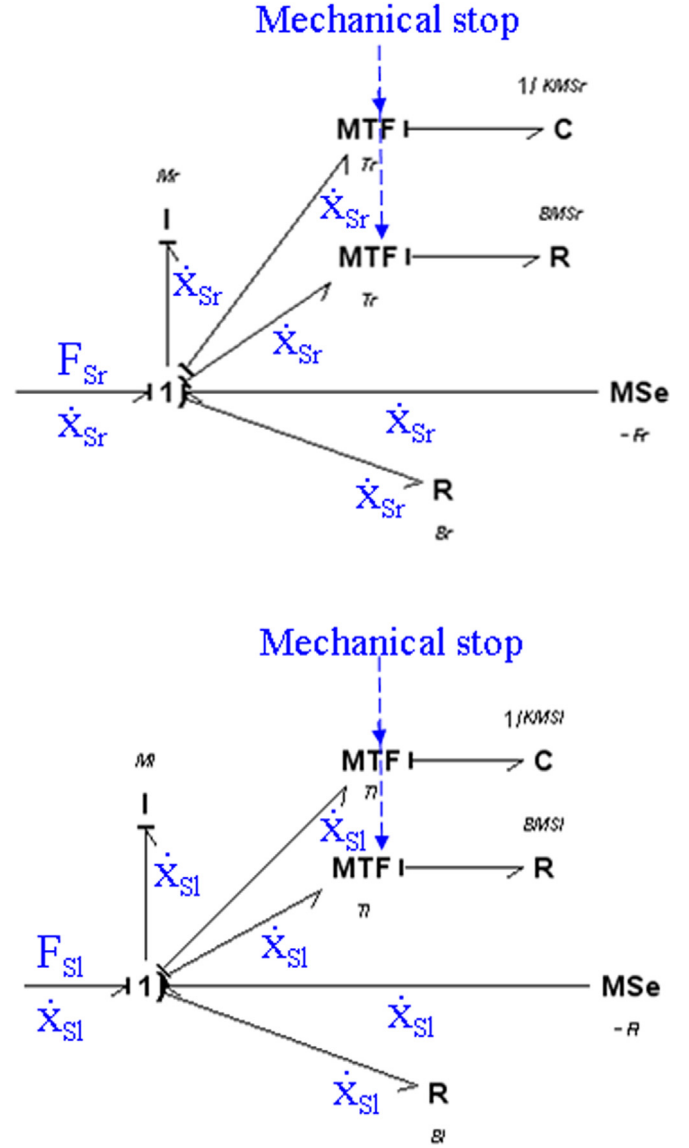


Fig. 6. Bond Graph model of Loads.

the both subsystems can be described by the following Eq. (9).

$$\begin{cases} M_r \cdot \ddot{x}_{Sr} = F_{Sr} - F_r - B_r \cdot \dot{x}_{Sr} - Tr^2 \cdot B_{MSr} \cdot \dot{x}_{Sr} - Tr^2 \cdot k_{MSr} \cdot x_{Sr} \\ M_l \cdot \ddot{x}_{Sl} = F_{Sl} - F_l - B_l \cdot \dot{x}_{Sl} - Tl^2 \cdot B_{MSl} \cdot \dot{x}_{Sl} - Tl^2 \cdot k_{MSl} \cdot x_{Sl} \end{cases} \quad (9)$$

Using Eq. (9), it is shown that the Bond Graph model of each load part subsystem can be represented by resistors dissipating free energy i.e. viscous friction ($R:B_r$, $R:B_l$), storage elements i.e. masses of the right and left loads ($I:M_r$, $I:M_l$), and two modulated source elements i.e. the Coulomb friction forces ($MSr:F_r$, $MSl:F_l$). Furthermore, mechanical stops are modeled by a C element ($C:1/k_{MSr}$) and a R element ($R:B_{MSr}$) modulated by a MTF element equal to 1 when the door reaches the mechanical stop and 0 otherwise. The obtained Bond Graph model is given in Fig. 6.

2.2.5. Reference model of the train door

Fig. 7, which is a concatenation of the previous Bond Graph submodels described above, leads to the global Bond Graph model of the train door mechatronic system. For each physical part, Table 1 gives the Bond Graph elements used for the system modeling and specifies their nominal reference values.

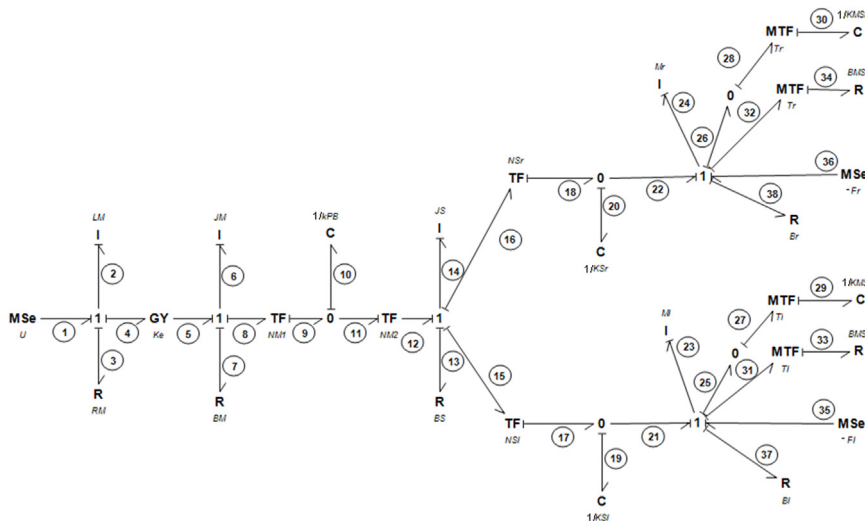


Fig. 7. Reference model of the train door mechatronic system.

Table 1
Description of the Bond Graph elements used to model the train door mechatronic system.

Physical part	Designation	Symbol	Bond Graph element	Nominal reference Value	Units
Motor (electrical part)	Motor resistance	<i>RM</i>	<i>R</i>	3.55 E-01	Ω
	Motor inductance	<i>LM</i>	<i>I</i>	1.50E-02	H
Motor (mechanical part)	Motor's back electromagnetic force constant	<i>ke</i>	<i>GY</i>	6.80E-02	$V \cdot s \cdot rad^{-1}$
	Viscous friction	<i>BM</i>	<i>R</i>	1.00E-05	$N \cdot s \cdot m^{-1}$
	Moment of inertia of the motor	<i>JM</i>	<i>I</i>	3.20E-04	$kg \cdot m^2$
Pulley-Belt	Reduction constant of the Pulley-Belt	<i>NM1</i>	<i>TF</i>	1.23E-01	-
	Reduction constant of the Pulley-Belt	<i>NM2</i>	<i>TF</i>	10	-
	Elasticity coefficient of the belt	<i>1/kPB</i>	<i>C</i>	1.00E-06	$m \cdot N^{-1}$
Spindle	Viscous friction of the inverse pitch spindle	<i>BS</i>	<i>R</i>	0.75E-03	$N \cdot s \cdot m^{-1}$
	Inertia of the inverse pitch spindle	<i>JS</i>	<i>I</i>	1.86E-04	$kg \cdot m^2$
	Rotation to linear transformation of the right side of the door	<i>NSr</i>	<i>TF</i>	1.27E-02	-
	Elasticity coefficient of the spindle-load (right side)	<i>1/kSr</i>	<i>C</i>	1.00E-06	$m \cdot N^{-1}$
Load (right)	Rotation to linear transformation of the left side of the door	<i>NSl</i>	<i>TF</i>	1.27E-02	-
	Elasticity coefficient of the spindle-load (left side)	<i>1/kSl</i>	<i>C</i>	1.00E-06	$m \cdot N^{-1}$
	Mass of the right side of the door	<i>Mr</i>	<i>I</i>	102	kg
	Coefficient of friction force (right side)	<i>BMSr</i>	<i>R</i>	9000	$N \cdot s \cdot m^{-1}$
Load (left)	Elasticity coefficient	<i>1/kMSr</i>	<i>C</i>	1E-05	$m \cdot N^{-1}$
	Viscous friction coefficient	<i>Br</i>	<i>R</i>	100	$N \cdot s \cdot m^{-1}$
	Mass of the left side of the door	<i>MI</i>	<i>I</i>	102	kg
	Coefficient of friction force (left side)	<i>BMSl</i>	<i>R</i>	9000	$N \cdot s \cdot m^{-1}$
	Elasticity coefficient	<i>1/kMSl</i>	<i>C</i>	1E-05	$m \cdot N^{-1}$
	Viscous friction coefficient	<i>Bl</i>	<i>R</i>	100	$N \cdot s \cdot m^{-1}$

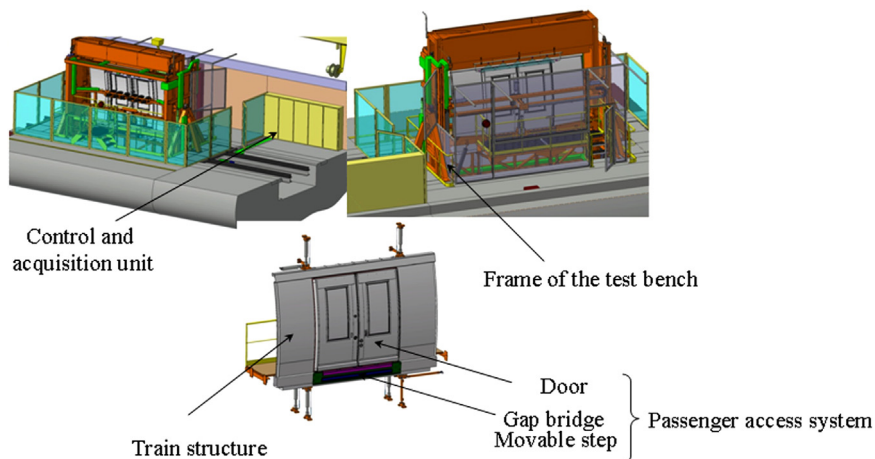


Fig. 8. The developed test bench for train door mechatronic system.

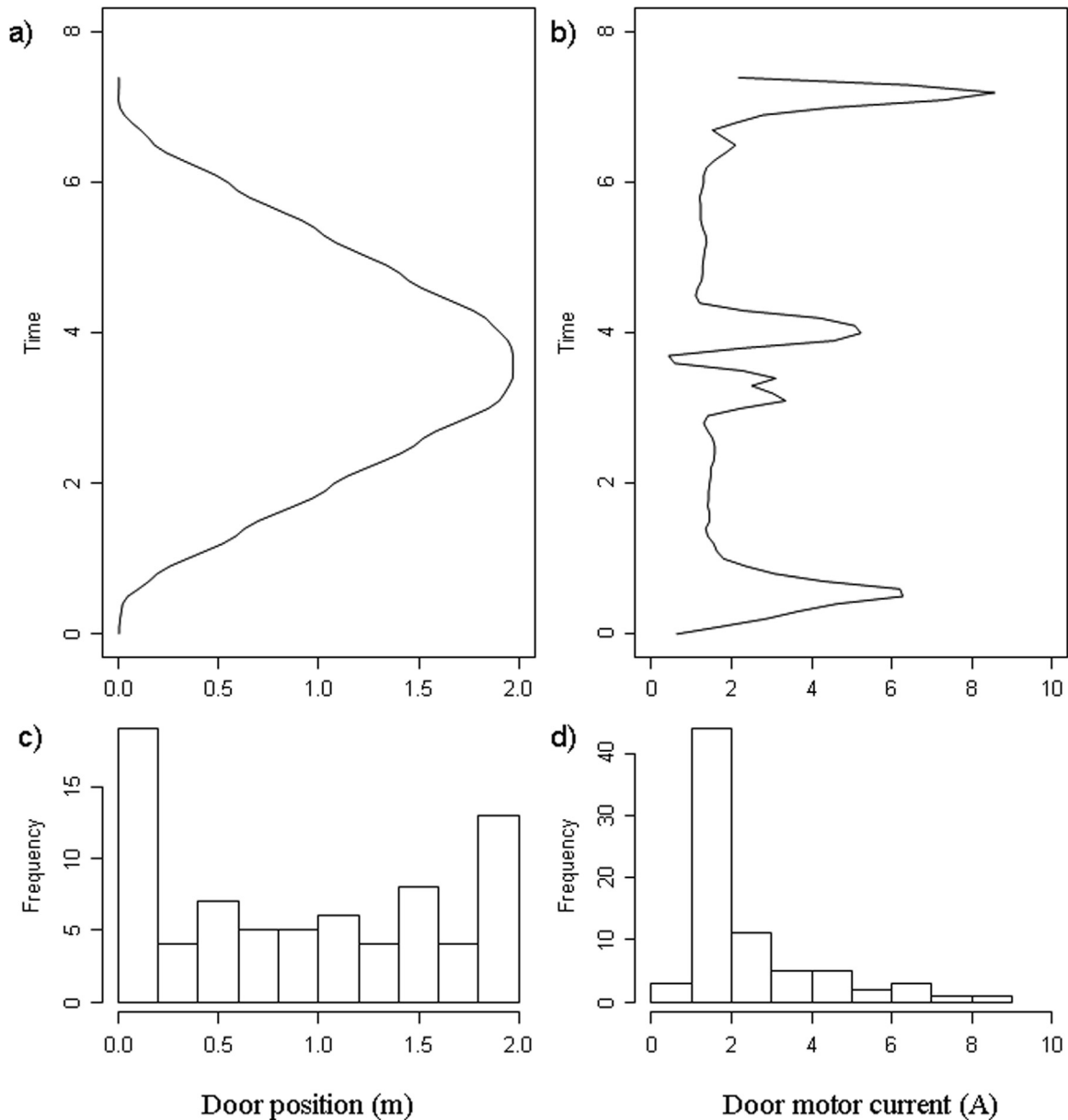


Fig. 9. Example of signals (a and b) and magnitude histograms for the door position and door motor current (c and d).

3. Validation of the reference Bond Graph model based onto real train door measurements

In order to validate the proposed reference model, measurement analyses have been made onto an industrial experimental test bench designed at the scale 1:1 by Bombardier Transport. This test bench was initially developed to test, to characterize and to detect early failures of train doors (Turgis et al., 2009; Cauffriez et al., 2013). One of the most advantages of this test bench is its ability to reproduce simultaneously all the mechanical, internal, and environmental stresses encountered while it is operating.

3.1. Description of the test bench

The test bench can be broken down into five sub-parts (Fig. 8):

1. The passenger access system, which is composed of three

independent mechanical sub-systems and the associated control equipment.

2. The structure representing the train in which the passenger access system operates in a worst-case configuration.
3. The frame of the test bench and its actuators, which includes the different electro-mechanical and electro-pneumatic devices used to evaluate the unit being tested.
4. The controller, for which the task is to control the actuators.
5. The control and acquisition unit, which controls the unit being tested, synchronizes the different test bench actuators, and centralizes data produced by the sensors placed on the passenger access system and on the test bench itself.

3.2. Measured and computed variables

For the door, the main variables are the relative position and door speed signals as well as the motor current and door closed

signals. More precisely, the relative position signal (i.e., the distance between the two leaves, which is between 0 and 2 m) is given by the train door's control unit with a sampling rate of 10 Hz, whereas the relative door speed signal is here calculated from the position signal using a smoothing procedure and derivation computation. It should run between 0 and about 0.8 m/s. The motor current signal which is obtained from the train door's control unit with a sampling rate of 10 Hz should run between 0 and 15 A. Finally, door closed signal is provided by the train door's limit switch with a sampling rate of 100 kHz. Then it is possible to obtain to the opening and closing instants. One can notice that the response time of the limit switch is between 30 and 100 ms.

3.3. Data mining for the exploratory statistical analysis of a mechatronic train door

To characterize the mechatronic train door system, it has been decided to process a Design of Experiments with an experimental campaign with normal operating conditions of the train door (i.e., without stresses). The experimental test bench recorded a multi-dimensional signal, in which the main components are related to the door position and the current intensity in the door motors i.e. for $V0=2$ components. Since a single opening/closing cycle of the train door was not sufficient, the experimental campaign consisted in a trial with a number of $D=160$ cycles of door opening and closing. Due to the recording technology used and the signal dynamics, the sampling frequency of the $V0$ time variables was not identical. It corresponded to 100 Hz for the door position and 10 Hz for the current intensity. The presence of doubtful values due essentially to Electromagnetic compatibility (EMC) disturbance was detected during the data analysis process.

Since it was necessary to verify that there was no time influence during the execution of the $D=160$ cycles for both $V0$ variables, two basic methods have been used to characterize and summarize recorded values: the first one was based on arithmetic mean (AM) and standard deviation (SD) values whereas the second one was the Membership Value Averages (MVA). From these methods, each multidimensional signal could be replaced with a new data set, which contained relatively synthetic indicators. These indicators are globally calculated for the entire signal duration and consist in generating arithmetic mean or Root Mean Square values and magnitude histogram frequency. Fig. 9a and b shows the time signals (a and b) of the door position and door motor current for one opening-closing cycle, whereas Fig. 9c and d illustrates the corresponding magnitude histograms (c and d) for the set of 160 cycles.

3.4. Comparison between experimental and simulation results

Simulations are performed using 20-Sim specific Bond Graph software (Kleijn, Grothuis & Differ, 2011). In order to compare experimental results with the simulation ones, the current signal is first considered. For the studied case, the train door opening/closing cycle has an average duration of 8 s. Fig. 10 shows the current for the proposed 20-sim Bond Graph model (dark line) and the real one measured on the test bench (red line).

After comparison, it should be mentioned that the overall shape of the motor current for the simulated Bond Graph model converges to the current of the real train mechatronic door although some discrepancies: the current of the Bond Graph model seems higher (3 A) compared to the current of the real system (2 A) for the translational motion of the door i.e. during 0.8–3.2 s time interval for the opening phase and 6.4–9 s time interval for the closing phase. There is also a small delay between the two current curves, the simulated signal being in phase-advanced in comparison with the real door current signal.

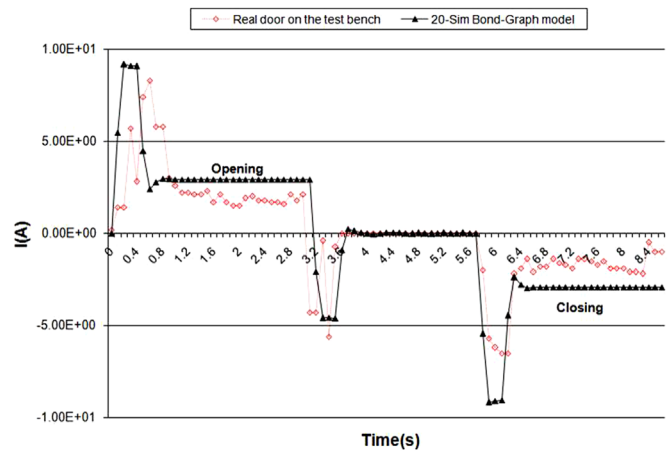


Fig. 10. Comparison of door motor current between a real door and the Bond Graph simulation. (For interpretation of the references to color in this figure, the reader is referred to the web version of this article.)

These differences may essentially be due to both the technical features of the elements constituting the door and the input control signal for the simulation model. First, the proposed characterization of the train door by the exploratory statistical analysis demonstrates a slight variation between opening and closing cycles of the door. Secondly, the simulated input control signal is theoretical and improvement could be obtained by using directly the door control signal of the train door i.e. by performing hardware in the loop process in a next step.

Given the overall shape of motor current and door position curves (see, respectively, Figs. 10 and 11), the reference model is consistent with the real train door. Henceforth, the next step is to build from this reference Bond Graph model a global model-based FDI for faults detection and isolation of the train door mechatronic system.

4. Global model-based FDI

4.1. Internal and external perturbations

In this section, the objective is to build a model based FDI in order to enable the detection and isolation respectively of:

1. A set of internal perturbations concerning either the motor, the Pulley-Belt, the spindle, or loads (right and left). Internal perturbations of the system features are therefore modeled through a variation of the reference nominal value.
2. A set of external perturbations whose experience feedback points out that the pushing of passengers and the

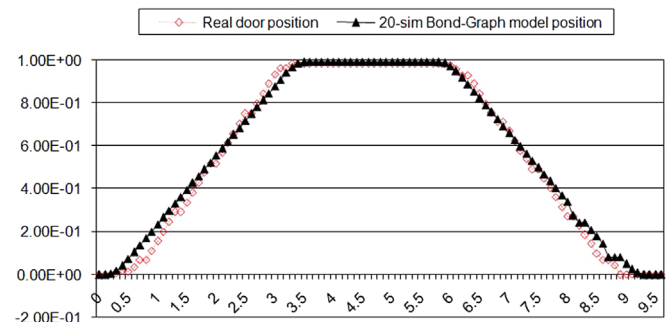


Fig. 11. Comparison of door position between a real door and the Bond Graph simulation.

superelevation of the train are the most influenced external factors (Cauffriez et al., 2013). Indeed, the superelevation of the train and the pushing of passengers lead to friction increase following Eq. (10).

$$F_{\text{external_perturbations}} = M \cdot g \cdot \mu_0 \cdot \sin(\alpha) + \mu_0 \cdot F_N \quad (10)$$

In Eq. (10), the first term corresponds to the friction increase due to a superelevation α , the mass M (i.e. M_r or M_l) representing the mass of doors, μ_0 the friction coefficient and g the acceleration of gravity. The second term of Eq. (10) refers to the pushing of passengers modeled by a normal force F_N .

4.2. Generation of fault indicators

Using the FDI algorithm proposed by (Merzouki et al., 2007; Ghoshal & Samanta, 2011), a list of Analytical Redundancy Relations (ARRs) along with the corresponding Fault Signature Matrix (FSM) can be generated. This allows detecting and isolating the possible faults present on the system. Following this algorithm, five number of flow sensors (D_f) have been installed within the system to match industrial requirements. In this algorithm, the first step is to build the Bond Graph model in preferred integral causality as shown in Fig. 12. Then, all the storage elements are to be brought under preferred differential causality with sensor causality inversion, if necessary, in order to derive the ARRs (see Fig. 13).

It is to be noted that for an observable system with none unresolved algebraic loops, the number of ARR generated is equal to the number of detectors on the reference Bond Graph model. Therefore five ARRs of the train door mechatronic system are given by Eqs. (11)–(15).

ARR₁:

$$U - L_M \frac{di}{dt} - R_M \cdot i - k_e \cdot \frac{d\theta_M}{dt} = 0 \quad (11)$$

ARR₂:

$$\begin{aligned} k_e \cdot i - J_M \cdot \frac{d^2\theta_M}{dt^2} - B_M \cdot \frac{d\theta_M}{dt} - N_{M1} \cdot N_{M2} \cdot \left(J_S \cdot \frac{d^2\theta_{PB}}{dt^2} + B_S \cdot \frac{d\theta_{PB}}{dt} \right) \\ - N_{M1} \cdot N_{M2} \cdot N_{Sr} \cdot \left\{ M_r \cdot \frac{d^2x_{Sr}}{dt^2} + (Br + Tr^2 \cdot B_{MSr}) \cdot \frac{dx_{Sr}}{dt} + Tr^2 \cdot k_{MSr} \cdot x_{Sr} + Fr \right\} \\ - N_{M1} \cdot N_{M2} \cdot N_{Sl} \cdot \left\{ M_l \cdot \frac{d^2x_{Sl}}{dt^2} + (Bl + Tl^2 \cdot B_{MSl}) \cdot \frac{dx_{Sl}}{dt} + Tl^2 \cdot k_{MSl} \cdot x_{Sl} + Fl \right\} = 0 \end{aligned} \quad (12)$$

ARR₃:

$$\begin{aligned} \frac{N_{M2}}{k_{PB}} \cdot \left\{ J_S \cdot \frac{d^3\theta_{PB}}{dt^3} + B_S \cdot \frac{d^2\theta_{PB}}{dt^2} \right\} + \frac{N_{M2} \cdot N_{Sr}}{k_{PB}} \\ \cdot \left\{ M_r \cdot \frac{d^3x_{Sr}}{dt^3} + (Br + Tr^2 \cdot B_{MSr}) \cdot \frac{d^2x_{Sr}}{dt^2} + Tr^2 \cdot k_{MSr} \cdot \frac{dx_{Sr}}{dt} + \frac{dFr}{dt} \right\} \\ + \frac{N_{M2} \cdot N_{Sl}}{k_{PB}} \cdot \left\{ M_l \cdot \frac{d^3x_{Sl}}{dt^3} + (Bl + Tl^2 \cdot B_{MSl}) \cdot \frac{d^2x_{Sl}}{dt^2} + Tl^2 \cdot k_{MSl} \cdot \frac{dx_{Sl}}{dt} + \frac{dFl}{dt} \right\} \\ - N_{M1} \cdot \frac{d\theta_M}{dt} + \frac{1}{N_{M2}} \cdot \frac{d\theta_{PB}}{dt} = 0 \end{aligned} \quad (13)$$

ARR₄:

$$\begin{aligned} N_{Sr} \cdot \frac{d\theta_{PB}}{dt} - \frac{dx_{Sr}}{dt} - \frac{1}{k_{Sr}} \\ \cdot \left\{ M_r \cdot \frac{d^3x_{Sr}}{dt^3} + (Br + Tr^2 \cdot B_{MSr}) \cdot \frac{d^2x_{Sr}}{dt^2} + Tr^2 \cdot k_{MSr} \cdot \frac{dx_{Sr}}{dt} + \frac{dFr}{dt} \right\} = 0 \end{aligned} \quad (14)$$

ARR₅:

$$\begin{aligned} N_{Sl} \cdot \frac{d\theta_{PB}}{dt} - \frac{dx_{Sl}}{dt} - \frac{1}{k_{Sl}} \\ \cdot \left\{ M_l \cdot \frac{d^3x_{Sl}}{dt^3} + (Bl + Tl^2 \cdot B_{MSl}) \cdot \frac{d^2x_{Sl}}{dt^2} + Tl^2 \cdot k_{MSl} \cdot \frac{dx_{Sl}}{dt} + \frac{dFl}{dt} \right\} = 0 \end{aligned} \quad (15)$$

The system is structurally controllable/observable if and only if two conditions are satisfied (Loureiro, Merzouki & Ould Bouama, 2012):

1. There is a causal path connecting a source/detector to each I and C element in integral causality.
2. All I and C elements accept derivative causality. If the latter is not completely respected, dualization of the source/detector is required to put all the I and C elements in derivative causality.

From Figs. 12 and 13, both previously cited conditions are satisfied and therefore the system is structurally observable. Once the list of ARRs is generated, the fault signature matrix can be build by deducing the signature of the system components on each residual. The corresponding fault signature matrix of the mechatronic system is given in Table 2 (F_d stands for fault detectability and I for fault isolability). A “one” value on F_d and I columns means that fault of the corresponding components are detectable and isolable. The presence of one value of ARR _{i} column shows the influence of the corresponding components on the residual dynamics.

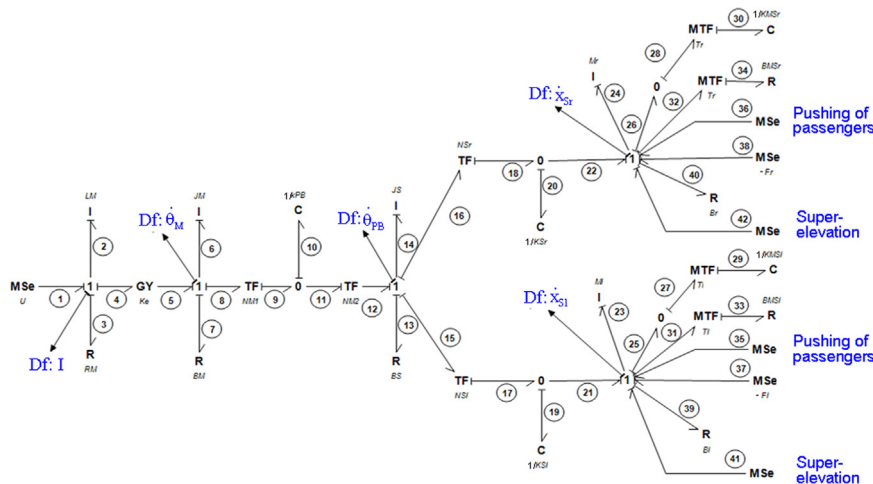


Fig. 12. Reference Bond Graph model of the train door mechatronic system in integral causality, with external perturbations.

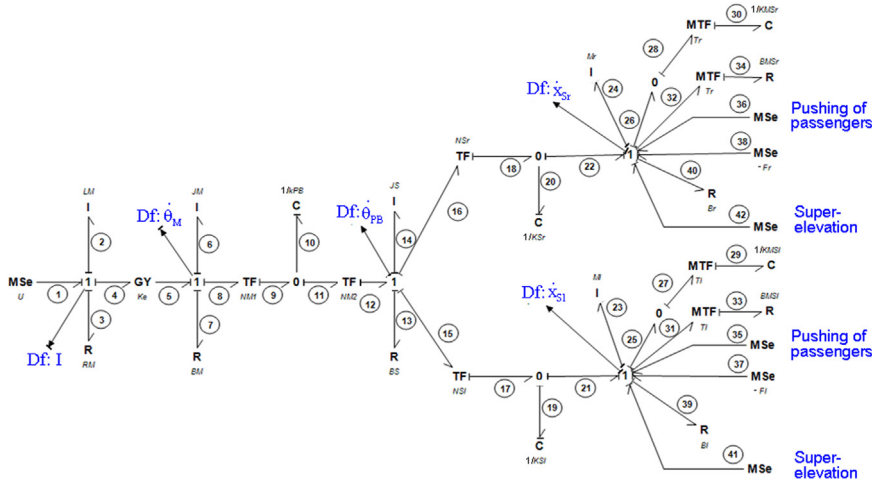


Fig. 13. Reference Bond Graph model of the train door mechatronic system in derivative causality, with external perturbations.

5. FDI simulation results

The purpose of the following simulations is to study the influence of internal and external perturbations on the various system signals in order to detect and isolate faults. Study of internal perturbations is willfully restricted to the motor, the pulley belt and the spindle since these perturbations appear to be the most frequent as demonstrated in (Turgis et al., 2009; Cauffriez et al., 2013). Internal perturbations are modeled by a variation of the reference nominal value of the train door mechatronic system. As the applied force on the door is not measured in our configuration, the fault detection is only observable during the slip mode i.e. when the door moves. In this case, the stick mode (i.e. when the door does not move) cannot be diagnosed. This stick mode is represented by blue areas on Figs. 14–20. Furthermore, to better distinguish stick and slip modes, the input voltage source U (Control_signal) used to move the door and the motor current (I_{motor}) are represented for all the corresponding figures. From Fig. 10, it is obvious that the diagnosis must be favored in the slip mode which corresponds to the steady state of the curve.

5.1. Study of internal perturbations

Internal faults for the motor are mostly due to inductance, resistance alteration or perturbation of the electromotive force

Table 2
Fault signature matrix.

Physical part	Symbol	ARR1	ARR2	ARR3	ARR4	ARR5	F_d	I
Motor (electrical part)	RM	1	0	0	0	0	1	0
	LM	1	0	0	0	0	1	0
Motor (mechanical part)	ke	1	1	0	0	0	1	1
	BM	0	1	0	0	0	1	0
	JM	0	1	0	0	0	1	0
Pulley-Belt	$NM1$	0	1	1	0	0	1	0
	$NM2$	0	1	1	0	0	1	0
	kPB	0	0	1	0	0	1	1
Spindle	BS	0	1	1	0	0	1	0
	JS	0	1	1	0	0	1	0
	NSR	0	1	1	1	0	1	0
	kSR	0	0	0	1	0	1	1
	NSI	0	1	1	0	1	1	0
Load (right)	kSL	0	0	0	0	1	1	1
	MR	0	1	1	1	0	1	0
	BR	0	1	1	1	0	1	0
Load (left)	ML	0	1	1	0	1	1	0
	BL	0	1	1	0	1	1	0

constant. Figs. 14 and 15 illustrate residual ARR1 to ARR5 for $a+1\%$ variation of the inductance L_M and the resistance R_M of the motor. As predicted in Table 2, the simulation result clearly shows that the residual ARR1 brings the capability to detect a L_M or R_M fault immediately. The shape of residual ARR1 allows distinguishing respectively the faults due to L_M (see Fig. 14) and R_M (see Fig. 15).

Fig. 16 depicts the residual signals ARR1 to ARR5 for $a+1\%$ variation of the motor's back electromagnetic force constant ke . Result shows that ARR1 and ARR2 are sensitive to this fault which matches the fault signature given in Table 2. Contrarily to previous cases, a ke motor fault can be not only detected but also isolated.

For the Pulley-Belt, internal faults result from variation of the elasticity coefficient of the belt: Fig. 17 illustrates the simulation result for $a+1\%$ variation of the $1/kpb$ elasticity coefficient of the belt. This result confirms Table 2 failure signature which means that this perturbation can be detected and isolated with residual ARR3.

As shown in Fig. 18, alteration of $+1\%$ of the linear transformation of the right side of the door NsR impacts residual ARR2, ARR3, ARR4 as predicted in Table 2.

5.2. Study of external perturbations

Experience feedback points out that the pushing of passengers and the superelevation of the train are the most influenced external factors since they lead to a friction increase of the door (Turgis et al., 2009; Cauffriez et al., 2013). To focus on this problem, a transient variation of the system friction is simulated.

5.2.1. Pushing of passengers

The passengers pushing perturbations correspond to a force applied on the door which releases as soon as the door opens because passengers move away from it. The passengers' pushing is modeled by Eq. (16). In this equation, A_N is the force amplitude imposed by the passengers pushing and $h(t)$ is the function modeling its activation (see the curve "Pushing of passengers" in Fig. 19).

$$FN = AN \cdot h(t) \quad (16)$$

Fig. 19 reveals that residuals ARR2 to ARR5 are sensitive to this fault. Therefore it is possible to isolate this fault from internal perturbations. One can observe that the residual signal ARR3 clearly exhibits a higher noise level than the one encountered in the other residuals which is not the case for the other experiments. This phenomenon is related to a numerical derivative computation in the algorithm.

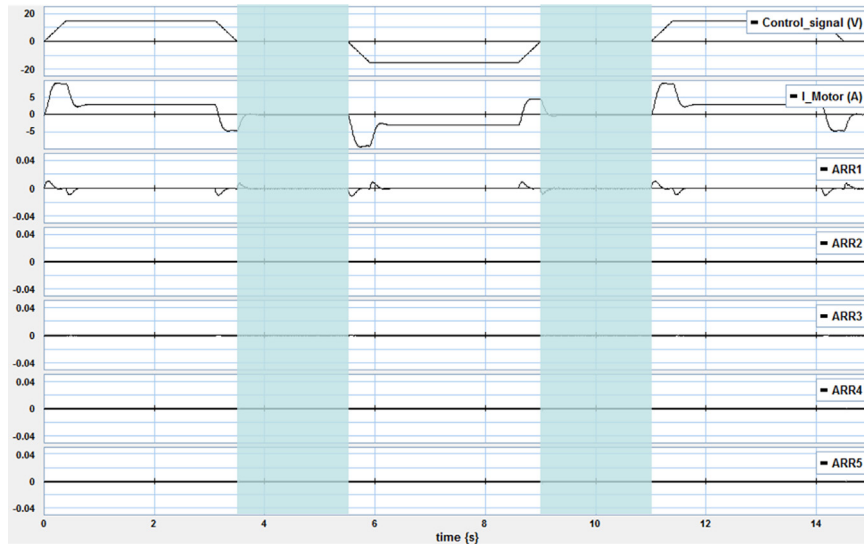


Fig. 14. Residual value 1 for $a+1\%$ variation of L_M nominal reference value.

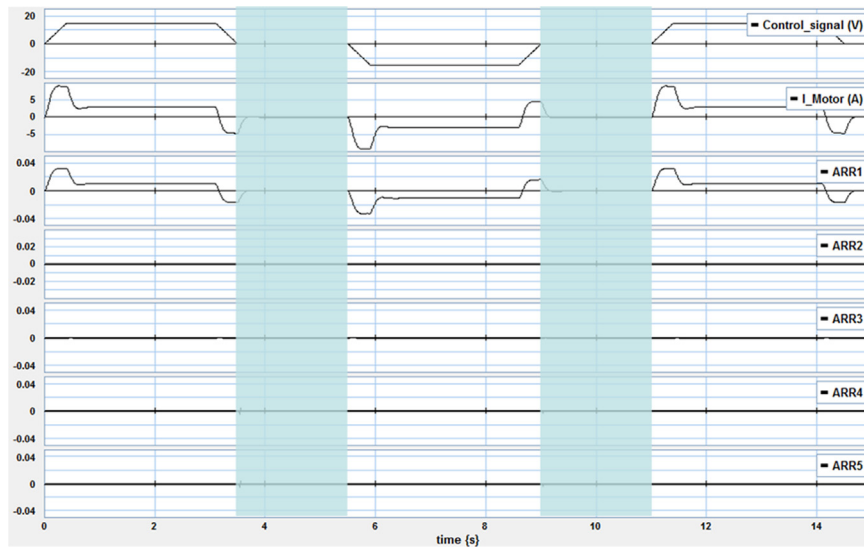


Fig. 15. Residual value 1 for $a+1\%$ variation of R_M nominal reference value.

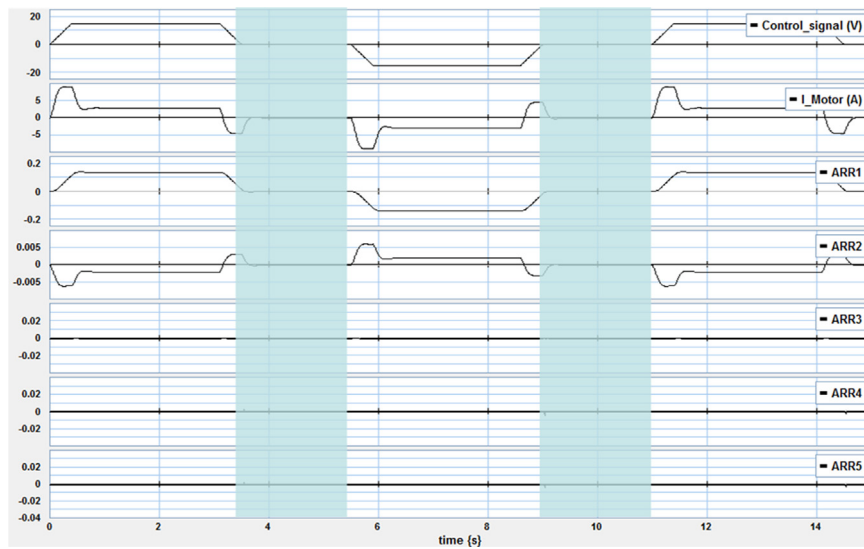


Fig. 16. Residual value 1 and 2 for $a+1\%$ variation of k_e motor reference value.

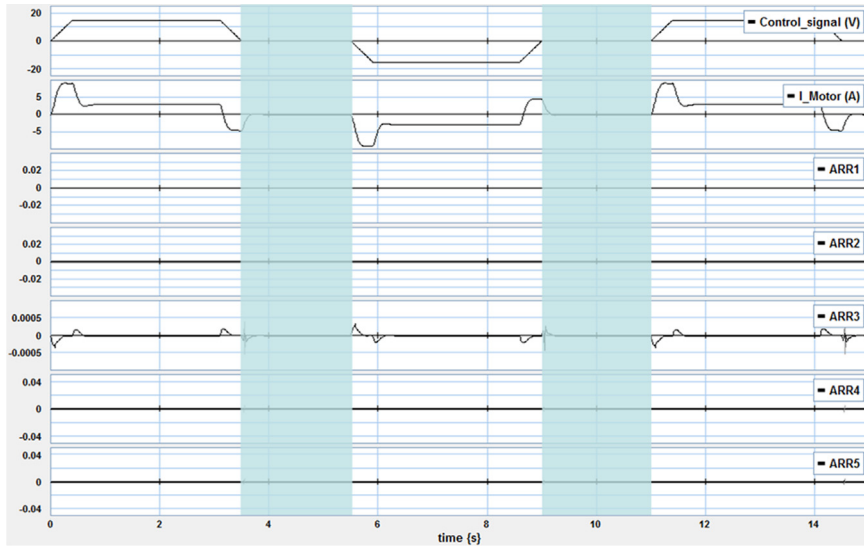


Fig. 17. Residual value 3 for $a+1\%$ variation of $1/kpb$ elasticity coefficient of the belt.

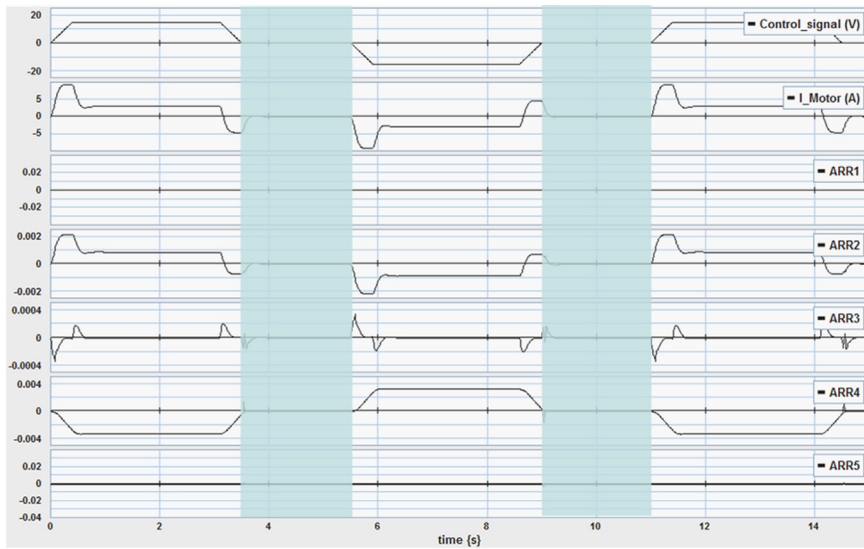


Fig. 18. Residual values 2, 3 and 4 for $a+1\%$ variation of the linear transformation of the right side of the door NsR .

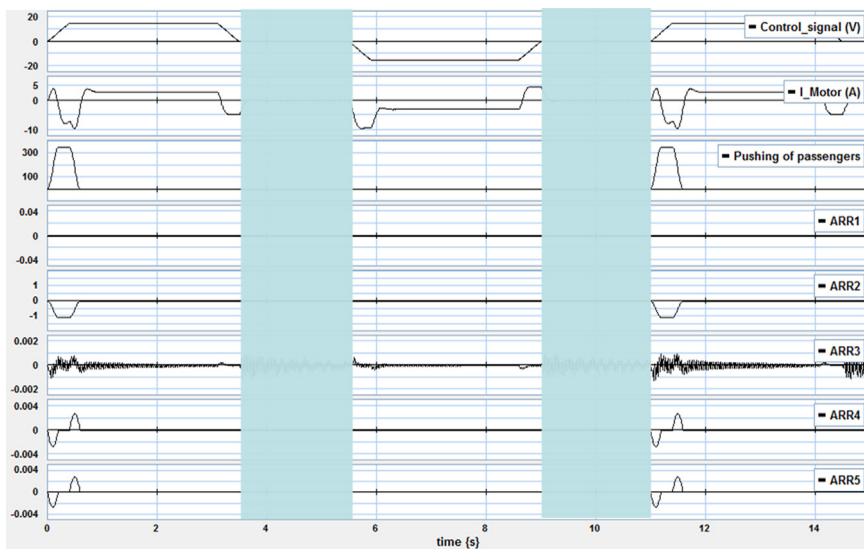


Fig. 19. Residual values 2, 3, 4 and 5 for passengers pushing.

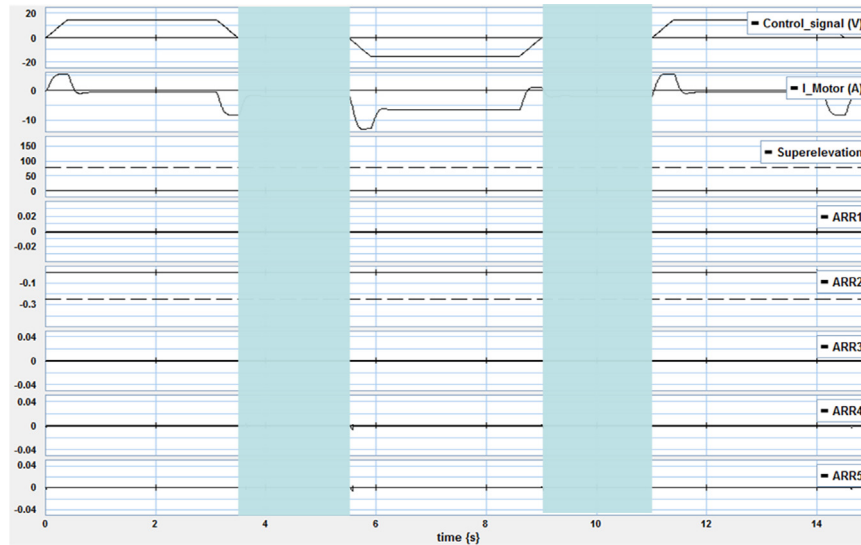


Fig. 20. Residual value 2 for a super-elevation of 0.174 rad.

5.2.2. Superelevation

The superelevation conduces to a tilting of the door which perturbs the normal conditions of door use. More precisely this tilting induces a friction force which is function of the tilt angle perturbation α . It should be noted that this perturbation is active during the time that the train is stopped in station. This phenomenon is modeled by following equation:

$$F_s = M \cdot g \cdot \mu_0 \cdot \sin(\alpha) \quad (17)$$

where M corresponds to the right or left M_r or M_l masses of the door, g is the gravity, μ_0 the friction coefficient and α the tilt angle perturbation.

The simulation result for the super-elevation perturbation is represented by a dashed line at Fig. 20. Contrarily to the previous case, it can be seen that this perturbation can be detected only with residual ARR2. This result is logical when looking forward Eq. (12)–(15) as ARR2 is equivalent to a sum of forces whereas ARR3 to ARR5 correspond to a sum of derivative forces. Consequently, the super-elevation perturbation assumed to be constant cannot be detected using residuals ARR3 to ARR5.

6. Conclusion

In this paper, a system reference model using Bond Graph formalism has been first proposed to characterize the behavior of a train door mechatronic system in normal operating mode and was validated after comparison with experimental measurements on a test bench.

The second step of this study has been to build a global model-based FDI in order to detect a set of internal perturbations (motor, Pulley-Belt, spindle, right or left loads) and external perturbations (pushing of passengers, super-elevation) of the train door mechatronic system. The system reference model has therefore been set in preferred derivative causality to deduce the Analytic Redundancy Relations ARR. These ARR relations have been used to construct the theoretical Fault Signature Matrix (FSM) in order to simulate scenario of faults detection.

Thus, the next step was the characterization of residuals due to internal door failures and allowed to verify the proposed theoretical fault signature matrix for the train door mechatronic system. Finally, residuals computations have also been exploited for some external perturbations like passengers pushing and super-elevation

problems demonstrating the ability of the proposed diagnostic model to face such a problem. Future work is in progress to develop such diagnosis in real-time on board.

References

- Akrad, A., Hilarait, M., & Diallo, D. (2011). Design of a fault-tolerant controller based on observers for a PMSM drive. *IEEE Transaction on Industrial Electronics*, 58(4), 1416–1427.
- Amerongen, J. Van (2003). Mechatronic design. *Mechatronics*, 13(10), 1045–1066.
- Blanke, M., Kinnaert, M., Lunze, J., & Staroswiecki, M. (2006). *Diagnosis and fault-tolerant control-design schemes, algorithms, and tools* (2nd ed.). Heidelberg: Springer-Verlag.
- Borutzky, W., Dauphin-Tanguy, G., & Thoma, J. U. (1995). Advances in Bond Graph modelling: theory, software, applications. *Mathematics and Computers in Simulation*, 39(5–6), 465–475.
- Borutzky, W. (2011). *Bond Graph of engineering systems-theory, applications and software support*. New York: Springer.
- Cauffriez, L., Loslever, P., Caouder, N., Turgis, F., & Copin, R. (2013). Robustness study and reliability growth based on exploratory design of experiments and statistical analysis: case study using a train door test bench. *International Journal of Advanced Manufacturing Technology*, 66, 27–44. <http://dx.doi.org/10.1007/s00170-012-4303-0>.
- Chen, J., & Patton, R. J. (1999). *Robust model-based fault diagnosis for dynamic systems*. Boston: Kluwer Academic Publishers.
- Chun, W. H., Speyer, J. L., & Chen, R. H. (2001). A decentralized fault detection filter. *ASME The Journal of Dynamic Systems, Measurement, and Control*, 123.
- Dassanayake, H., Roberts, C., Goodman, C. J., & Tobias, A. M. (2009). Use of parameter estimation for the detection and diagnosis of faults on electric train door systems. *Proceedings of the Institution of Mechanical Engineers Part O: Journal of Risk and Reliability*, 223(4), 271–278.
- Ding, S. X. (2008). *Model-based fault diagnosis techniques—design schemes, algorithms, and tools*. London: Springer-Verlag.
- Gawthrop, P. J. (1991). Bond Graphs: a representation for mechatronic systems. *Mechatronics*, 1(2), 127–156.
- Ghoshal, S. K., & Samanta, S. (2011). Robust fault diagnosis and prognostics of a hoisting mechanism: a simulation study. *International Journal of Engineering Science and Technology IJEST*, 3(2), 962–980.
- Henry, D. (2013). Robust control and linear parameter varying approaches. *Lecture Notes in Control and Information Sciences*, 437, 125–180.
- Isermann, R. (2005). Model-based fault-detection and diagnosis—status and applications. *Annual Reviews in Control*, 2005(29), 71–85.
- Isermann, R. (2006). *Fault diagnosis systems—an introduction from fault detection to fault tolerance*. Berlin Heidelberg: Springer-Verlag.
- Jang, J. O., & Jeon, G. J. (2000). A parallel neuro-controller for DC motors containing nonlinear friction. *Neurocomputing*, 30(1–4), 233–248.
- Keliris, C., Polycarpou, M., & Parisini, T. (2015). A robust nonlinear observer-based approach for distributed fault detection of input–output interconnected systems. *Automatica*, 53, 408–415.
- Kleijn, C., Grothuis, M.A., Differ, H.G. (2011). 20-sim 4.2 Reference manual, Control products B.V.
- Li, W., Gui, W.H., Xie, Y.F. & Ding, S.X. (2009). Decentralized fault detection system design for large-scale interconnected systems. In: *Proceedings of IFAC Safe-process*. Barcelona.

- Loureiro, R., Merzouki, R., & Bouamama, Ould (2012). Bond Graph model based on structural diagnosability and recoverability analysis: application to intelligent autonomous vehicles. *IEEE Transactions on Vehicular Technology*, 61(3), 986–997.
- Menhaged, K., Yamé, J.J., & Aubrun C. (2010) An Improved Robust Adaptive Observer for Actuator Fault Detection. In: *Proceedings of the 11th International conference on Control Automation Robotics & Vision (ICARV)*, pp. 1322–1328.
- Merzouki, R., Medjaher, K., Djeziri, M. A., & Ould-Bouamama, B. (2007). Backlash fault detection in mechatronic system. *Mechatronics*, 17(6), 299–310.
- Mezghanni, D., Andoulsi, R., Mami, A., & Dauphin-Tanguy, G. (2007). Bond Graph modelling of a photovoltaic system feeding an induction motor-pump. *Simulation Modelling Practice and Theory*, 15(10), 1224–1238.
- Nazari, R., Seron, M. M., & De Doná, J. A. (2013). Fault-tolerant control of systems with convex polytopic linear parameter varying model uncertainty using virtual-sensor-based controller reconfiguration. *Annual Reviews in Control*, 37(1), 146–153.
- Niu, G., Zhao, Y., Defoort, M., & Pecht, M. (2015). Fault diagnosis of locomotive electro-pneumatic brake through uncertain Bond Graph modeling and robust online monitoring. *Mechanical Systems and Signal Processing*, 50–51, 676–691.
- Ould Bouamama, B., Medjaher, K., Bayart, M., Samantaray, A. K., & Conrard, B. (2005). Fault detection and isolation of smart actuators using Bond Graphs and external models. *Control Engineering Practice*, 13(2), 159–175.
- Paynter, H. M. (1959). Hydraulics by analog and electronic model of a pumping plant. *Journal of Boston Society of Civil Engineers*, 46(6), 197–219.
- Patton, R. J., Franck, P. M., & Clark, R. N. (2000). *Issues of fault diagnosis in dynamic systems*. New-york: Springer-Verlag Berlin Heidelberg ISBN-10:3540199683.
- Ponsart, J. C., Theilliol, D., & Aubrun, C. (2010). Virtual sensors design for active fault tolerant control system applied to a winding machine. *Control Engineering Practice*, 18(9), 1037–1044.
- Rosenberg, D. W., Balance, D. J., & Gawthrop, P. J. (1995). Design and implementation of a Bond Graph observer for robot control. *Control Engineering Practice*, 3(10), 1447–1457.
- Rosenberg, R. C., & Karnopp, D. C. (1972). A definition of the Bond Graph language. *Journal of Dynamic Systems, Measurement, and Control*, 94(3), 179–182.
- Samantaray, A. K., Medjaher, K., Ould Bouamama, B., Staroswiecki, M., & Dauphin-Tanguy, G. (2006). Diagnostic Bond Graphs for online fault detection and isolation. *Simulation Modelling Practice and Theory*, 14(3), 237–262.
- Samantaray, A. K., & Ghoshal, S. K. (2008). Bicausal Bond Graphs for supervision: from fault detection and isolation to fault accommodation. *Journal of The Franklin Institute*, 345(1), 1–28.
- Svard, C., Nyberg, M., Frisk, E., & Krysander, M. (2014). Data-driven and adaptive statistic residual evaluation for fault detection with an automotive application. *Mechanical Systems and Signal Processing*, 45, 170–192.
- Turgis, F., Copin, R., Loslever, P., Cauffriez, L., & Caouder N. (2009). Design of a testing bench for simulating tightened-up operating conditions of train's passenger access. In: *Proceedings of ESREL*. Prague, Czech Republic, 21-23 September.
- Varga, A., & Ossmann, D. (2014). LPV model-based robust diagnosis of flight actuator faults. *Control Engineering Practice*, 31, 135–147.
- Venkatasubramanian, V., Rengaswamy, R., & Kavuri, S. N. (2003). Review of process fault detection and diagnosis. *Computers and Chemical Engineering*, 27, 293–311.
- Yan, X. G., & Edwards, C. (2007). Robust decentralized actuator fault detection and estimation for large-scale systems using sliding mode observer. *International Journal of Control*, 81, 591–606.
- Youssef, A. B., El Khil, S. K., & Slama-Belkhdja, I. (2013). State observer-based sensor fault detection and isolation, and fault tolerant control of a single-phase PWM rectifier for electric railway traction. *IEEE Transactions on Power Electronics*, 28(12), 5842–5853.

Laurent Cauffriez has a Ph.D. degree in control for industrial and human systems from the University of Valenciennes (France), and is an Associate habilitated Professor at the ENSIAME in Valenciennes (The National School of Engineering for Computer Science, Automation, Mechanics and Electronics). He is a member of the LAMIH research laboratory (Laboratory of Industrial and Human Automation, Mechanics, and Computer Science), which is associated with the CNRS (National Center for Scientific Research). He teaches courses on reliability and safety, the

simulation of automated production systems, and production management. His research centers on dependability and fault detection in complex systems and is applied principally to production systems, distributed control/command systems and railway systems. He is the editor of one book and the author of two chapters in a second one, as well as the author of around fifty papers in international journals and conferences.

Sébastien Grondel received the M.S. and Ph.D. degrees in electrical and acoustical Engineering from Valenciennes University, France, in 1997 and 2000, respectively. Between 2001 and 2010, he worked as a research Associate at the Electronic, Microelectronic and Nanoelectronic department of Valenciennes University, focusing on health monitoring of aeronautic structures using elastic guided waves and multi-array piezoelectric transducers. Since 2011, he is a Professor in the same department and teacher at the engineering school ENSIAME. His current research activities include modeling and control of macro- and micro- mechatronic systems through the use of the Bond Graph methodology. He contributes on the design and development of a nano flying insect called "OVMI" as well as on new ionic polymers actuators. He has authored more than 50 published journal and conference papers related to smart material, ultrasonic and mechatronic. He is also a member of the French Acoustical (SFA) and Electronic Electrotechnic and Automatic (EEA) Societies.

Pierre Loslever has a Ph.D. degree in control for industrial and human systems from the University of Valenciennes (France), and is a Professor in Valenciennes at the engineering school ENSIAME. He is a member of the LAMIH research laboratory (Laboratory of Industrial and Human Automation, Mechanics, and Computer Science). He primarily teaches courses in data analysis related domains, such as Signals and Systems, Statistics, Maintenance or Quality management. His research mainly focuses on human component systems studies with aspects such as ergonomics or biomechanics, yielding about sixty papers in international journals.

Christophe Aubrun received the Doctorat d'Université in 1993 from the University Henri Poincaré, Nancy I, France. Since 2003 he is a full Professor at University Henri Poincaré, Nancy I, where he teaches Automatic Control. He has been the Director of the Institut Universitaire Professionnalis  in Electrical engineering and head of the department of Electrical Engineering of the Institut Universitaire de Technologie of Nancy. He is a member of the Research Centre In Automatic Control of Nancy (CRAN). His current research interests are focused on model-based fault diagnosis and fault tolerant with emphasis on networked control systems and continuous commissioning of building energy system.